α and ^{3}He production in the ^{7}Be + ^{28}Si reaction at near-barrier energies: Direct versus compound-nucleus mechanisms

O. Sgouros,[1] A. Pakou,[1,*] D. Pierroutsakou,[2] M. Mazzocco,[3,4] L. Acosta,[5,6] X. Aslanoglou,[1] Ch. Betsou,[1] A. Boiano,[2] C. Boiano,[7] D. Carbone,[8] M. Cavallaro,[8] J. Grebosz,[9] N. Keeley,[10] M. La Commara,[11,2] C. Manea,[4] G. Marquinez-Duran,[12] I. Martel,[12] N. G. Nicolis,[1] C. Parascandolo,[2] K. Rusek,[13] A. M. Sánchez-Benítez,[14,12] C. Signorini,[15] F. Soramel,[3,4] V. Soukeras,[1] C. Stefanini,[3] E. Stiliaris,[16] E. Strano,[3,4] I. Strojek,[10] and D. Torresi[3,4]

[1]*Department of Physics and HINP, The University of Ioannina, 45110 Ioannina, Greece*
[2]*INFN, Sezione di Napoli, via Cintia, 80126 Napoli, Italy*
[3]*Dipartimento di Fisica e Astronomia, Universita di Padova, via Marzolo 8, I-35131 Padova, Italy*
[4]*INFN - Sezione di Padova, via Marzolo 8, I-35131 Padova, Italy*
[5]*Instituto de Fisica, Universidad Nacional Autonoma de Mexico, Mexico D.F. 01000, Mexico*
[6]*INFN - Sezione di Catania, via S. Sofia 64, 95125 Catania, Italy*
[7]*INFN, Sezione di Milano, via Celoria 16, I-20133 Milano, Italy*
[8]*INFN Laboratori Nazionali del Sud, via S. Sofia 62, 95125 Catania, Italy*
[9]*The Henryk Niewodniczański Institute of Nuclear Physics (IFJ PAN), Kraków, Poland*
[10]*National Centre for Nuclear Research, ul. Andrzeja Sołtana 7, 05-400 Otwock, Poland*
[11]*Dipartimento di Scienze Fisiche, Università di Napoli "Federico II", via Cintia, I-80126 Napoli, Italy*
[12]*Departamento de Ciencias Integradas, Universidad de Huelva, E-21071 Huelva, Spain*
[13]*Heavy Ion Laboratory, University of Warsaw, Pasteura 5a, 02-093 Warsaw, Poland*
[14]*Centro de Física Nuclear da Universidade de Lisboa, 1649-003 Lisboa, Portugal*
[15]*INFN, LNL, viale dell'Universita 2, I-35020 Legnaro, Italy*
[16]*Institute of Accelerating Systems and Applications and Department of Physics, University of Athens, Athens, Greece*
(Received 19 July 2016; revised manuscript received 30 September 2016; published 28 October 2016)

The production of α and ^{3}He particles, the cluster constituents of ^{7}Be, in the ^{7}Be + ^{28}Si reaction was studied at three near-barrier energies, namely 13, 20, and 22 MeV. Angular distribution measurements were performed at each energy, and the data were analyzed in both statistical model and Distorted-Wave Born Approximation (DWBA) frameworks in order to disentangle the degree of competition between direct and compound channels. The energy evolution of the ratio of direct to total reaction cross section was mapped in comparison with similar data for ^{6}Li and ^{7}Li projectiles on a ^{28}Si target. The results indicate larger transfer contributions for collisions involving the mirror nuclei ^{7}Be and ^{7}Li than in the ^{6}Li case. Fusion cross sections were deduced, taking into account the α-particle cross sections due to compound-nucleus formation and particle multiplicities deduced from our statistical model framework. It was found that fusion is compatible with systematics and single-barrier penetration cross sections to within an uncertainty band of 10% to 20%. Indications of fusion hindrance for ^{7}Li and ^{7}Be compared to ^{6}Li, starting from the barrier and below it, are given. This hindrance is attributed to the existence of large transfer channels. Furthermore, the experimental results, analyzed in the DWBA framework, suggest ^{3}He and ^{4}He transfer as the dominant direct reaction mechanism.

DOI: 10.1103/PhysRevC.94.044623

I. INTRODUCTION

Investigations of collisions involving weakly bound projectiles at near-barrier energies create a very interesting field for studies of reaction mechanisms and channel coupling effects, since direct processes like transfer and breakup are enhanced in these systems [1–9]. In this respect several studies of inclusive and exclusive measurements of light reaction products have been undertaken. Large α yields have been observed for most of the weakly bound projectiles, either stable like ^{6,7}Li and ^{9}Be or radioactive like ^{6,8}He. Exclusive measurements have been reported, mainly for stable weakly bound projectiles, e.g., ^{6}Li on ^{28}Si [10], ^{59}Co [11–13], ^{208}Pb [14,15], ^{209}Bi [16], ^{6}He on ^{209}Bi [17], ^{7}Li on ^{28}Si [18], ^{58}Ni [19], ^{65}Cu [20], ^{93}Nb [21], and ^{208}Pb [15,22]. Relevant inclusive measurements for stable [23–26] as well as radioactive projectiles [27–33] display significant contributions from direct channels including breakup. Quantifying the energy evolution of the direct contribution to the total cross sections, the authors in Ref. [34] predict a significant direct contribution at the barrier of the order of 50% to 80% for ^{28}Si and ^{208}Pb targets, respectively. This prediction is supported by Coupled Reaction Channel (CRC) calculations [34]. The direct contribution, according to the prediction, is enhanced up to ~100% below the barrier while it is saturated to ~20% above the barrier. Since the degree of competition between compound and direct channels is related to the effect of the potential threshold anomaly (see, e.g., Refs. [35,36]) as well as to the fusion itself, knowledge of its evolution as a function of energy, projectile, and target is an important piece of information for an understanding of the question of the enhancement or suppression of fusion in

*Corresponding author: apakou@cc.uoi.gr

these systems. It should be noted that fusion cross section enhancements have been reported for various projectiles and targets (see, e.g., the measurements for $^{6}He + ^{209}Bi$ [37] and $^{7}Be + ^{58}Ni$ [38]). However, comprehensive measurements disentangling the direct from the compound contribution to the total cross section for $^{6,8}He$ on ^{238}U and ^{197}Au [39,40] and ^{7}Be on ^{238}U [41] show that fusion is not enhanced but follows rather closely a single-barrier penetration model prediction [42].

In this respect, we report here a detailed study of the light particle production in the $^{7}Be + ^{28}Si$ reaction, concentrating on the ^{4}He and ^{3}He cluster constituents of ^{7}Be, the first originating from both compound and direct mechanisms and the latter solely from direct processes. The proton rich ^{7}Be is a weakly bound radioactive nucleus, with a $^{4}He + ^{3}He$ cluster structure, mirror of the weakly bound stable ^{7}Li. The breakup threshold for ^{7}Be is 1.59 MeV, lower than the corresponding 2.47 MeV of ^{7}Li but similar to the 1.47 MeV of ^{6}Li. It is therefore an interesting point to investigate whether the behavior of ^{7}Be more resembles that of ^{6}Li or ^{7}Li. The above system was chosen because comprehensive studies already exist for the related systems $^{6,7}Li + ^{28}Si$. Angular distributions of α yields were reported previously in Refs. [18,23,24] for ^{6}Li and ^{7}Li, respectively, exhibiting very different shapes. While for ^{6}Li bell-shaped angular distributions are observed similar to those measured for ^{6}He on ^{209}Bi and ^{6}Li on ^{209}Bi in exclusive measurements, for ^{7}Li the distributions are continuous. It should also be noted that a large hindrance of the fusion cross sections for ^{7}Li compared to ^{6}Li was reported for the first time by Beck *et al.* for the $^{6,7}Li + ^{59}Co$ systems [43] and later by other authors for the same projectiles but for the following targets: ^{24}Mg [44], ^{28}Si [45,46], and ^{64}Zn [47]. In more detail, the reported ratios of ^{6}Li to ^{7}Li fusion cross sections exhibited an increasing trend approaching the barrier from higher to lower energies, according to some measurements, while the increasing behavior was obvious only well below the barrier for some other measurements. However, within the error bars all measurements were compatible and supported hindrance of fusion for ^{7}Li compared to ^{6}Li. An exception to this behavior was reported for the $^{6,7}Li + ^{209}Bi$ systems [48]. The hindrance of fusion for ^{7}Li compared to ^{6}Li was attributed to breakup by means of Continuum Discretized Coupled Channel (CDCC) calculations for $^{6,7}Li + ^{59}Co$ in Ref. [49]. The opposite behavior for a ^{209}Bi target was not, however, explained by the same calculations. Therefore, in principle by comparing in a phenomenological approach angular distributions of α-particle reaction products and fusion cross sections for ^{7}Be with those for ^{6}Li and ^{7}Li we could draw useful conclusions.

The goals of this work are

(1) to identify the extent of the competition between direct reactions and compound-nucleus formation as a function of energy, as well as to determine fusion cross sections;
(2) to initiate a constructive discussion as to the direct mechanisms involved, by comparisons between the ^{3}He and ^{4}He particle production cross sections in a DWBA framework;
(3) to investigate the similarity between ^{7}Be and ^{7}Li or ^{6}Li.

II. EXPERIMENTAL DETAILS

The ^{7}Be secondary beam was produced at the EXOTIC facility [50–54] at the Laboratori Nazionali di Legnaro (LNL), Italy by means of the In Flight (IF) technique and the $^{1}H(^{7}Li,^{7}Be)n$ reaction. A comprehensive description of the beam production is given in Ref. [33]. Details pertinent to this work are given below. The $^{7}Li^{3+}$ primary beam was delivered by the LNL-XTU Tandem Van de Graaff accelerator with an intensity of ∼150pnA and energies of 31 and 33 MeV. The primary beam was directed onto a 5 cm long gas cell with 2.2 μm thick Havar foil windows filled with H_2 gas at a pressure of ∼1000 mbar and a temperature of 93 K, corresponding to an effective thickness of 2 mg/cm^2. The ^{7}Be beam was produced at three energies, namely, 13, 20, and 22 MeV, the highest two being obtained by retuning the primary beam while the lowest was obtained via a degrader. The beam passed through two xy sensitive Parallel Plate Avalanche Counters (PPACs) located along the beam line 909 mm (PPAC$_A$) and 365 mm (PPAC$_B$) upstream of the secondary target then impinged on a 0.4 mg/cm^2 thick ^{28}Si target, the reaction products being recorded in the detector array of the EXOTIC facility, EXPADES [55,56]. The experimental setup, a schematic view of which is presented in Fig. 1, included six telescopes from EXPADES. Each telescope comprised ΔE and E double-sided silicon strip detectors (DSSSD), with thicknesses of ∼55 μm and 300 μm, respectively. Both modules had active areas of 64 × 64 mm^2 with 32 strips per side, orthogonally oriented to define 2 × 2 mm^2 pixels. Details of how the detector signals were handled may be found in Ref. [56]. The strips were short-circuited two by two, therefore the angular resolution was in principle ∼2° per angular position, considering a pointlike beam spot on target. Taking into account the finite dimensions of the beam spot, estimated from a reconstructed spectrum to be of the order of ∼1 cm, this resolution increases to ∼4°. The forward telescopes T1 and T6 were set at ±27°, T2 and T5 at ±69°, and T3 and T4 at ±111°, spanning the following angular ranges: ∼13° to 41° and ∼14° to 40° for the forward telescopes, ∼54° to 85° for the middle telescopes, and ∼96° to 126° for the backward telescopes. The telescopes were

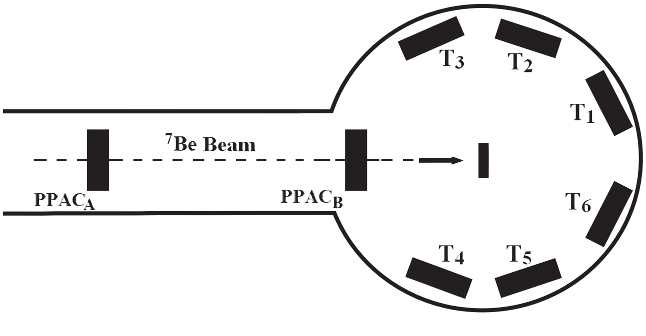

FIG. 1. Schematic view of the experimental setup, which includes six of the 8 modules of the EXOTIC array EXPADES [55,56]. Each module-telescope comprises two DSSSD detectors as explained in the text. Telescopes T1 and T6 were set at ±27°, T2 and T5 at ±69°, and T3 and T4 at ±111°, spanning the following angular ranges: ∼13° to 41° and ∼14° to 40° for the forward detectors, ∼54° to 85° for the middle telescopes, and ∼96° to 126° for the backward telescopes.

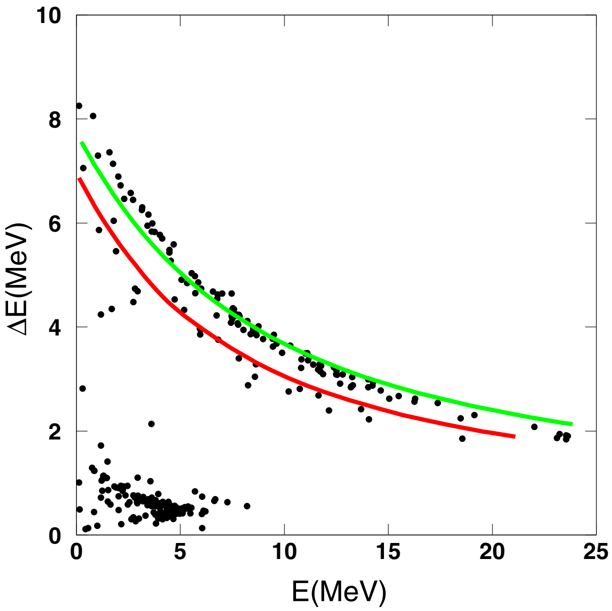

FIG. 2. Two-dimensional ΔE-E correlation plot for telescope T1, set at forward angles. Good separation between the ^{3}He and ^{4}He particles is observed. The solid lines represent kinematical simulations, presenting very good consistency with the data.

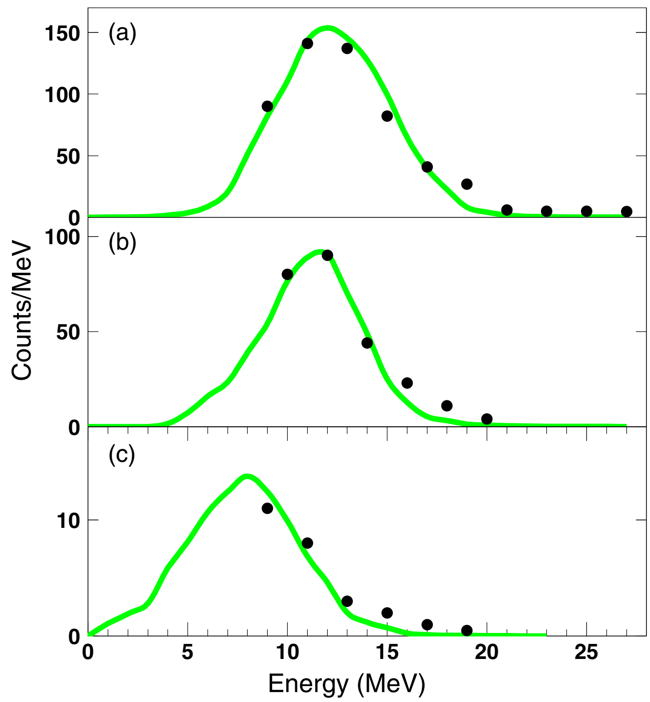

FIG. 3. Alpha energy spectra ($\Delta E + E$) for telescope T1 (at 27°) for the three bombarding energies (a) 22 MeV, (b) 20 MeV, and (c) 13 MeV. The solid line is a simulated spectrum taking into account both evaporation and direct mechanisms (see text and Fig. 4).

set at symmetrical positions to balance any beam divergence and to improve the statistics of the measurement. The trigger of the electronics was given by a signal created by the OR of the ΔE stage of the telescopes in coincidence with the PPAC signal set. The reaction products, ^{3}He and ^{4}He, were well separated by the ΔE-E technique, as may be seen in Fig. 2, where we present a two-dimensional correlation plot for one strip of telescope T1. The α and ^{3}He yields for each strip, detector, and projectile nergy, were obtained by putting appropriate windows on such two-dimensional plots. Representative one-dimensional α energy spectra ($\Delta E + E$) for telescope T1 are given in Fig. 3 for each projectile energy. Missing counts, due to the energy threshold of each telescope (ΔE thickness), were estimated via comparisons of experimental energy spectra with simulated ones.

For the simulations a Monte Carlo code was developed to describe the direct channels leading to the emission of α particles, namely the neutron pickup channel leading to ^{8}Be, the neutron stripping channel leading to ^{6}Be, and the ^{3}He-stripping channel. The breakup process was not considered as the cross section was estimated in preliminary CDCC calculations to be small. α-particle energy spectra for these processes were generated by this code, starting from angular distributions obtained in a DWBA approach, to be described below, for the production of ^{8}Be (^{4}He + ^{4}He) and ^{6}Be (^{4}He +2p). No theoretical calculation was performed for the ^{3}He stripping due to the lack of suitable spectroscopic factors. Tests adopting either specific angular distributions or isotropic ones gave similar energy spectra; therefore, in this particular case we proceeded with the assumption of an isotropic distribution. The appropriate transformations from the center-of-mass to the laboratory system were obtained going through the rest mass of the initial nucleus before breakup K, and a system K' moving in parallel to K, according to the prescription of Olimov *et al.* [57]. The final energy spectrum originating from direct processes was obtained by summing the three energy spectra normalized to the calculated cross sections. Finally, direct and compound-nucleus spectra were summed under various assumptions of the ratio of direct to compound-nucleus contributions and were fitted to the data. The compound-nucleus calculations were performed with the code PACE2 [58] taking into account as level density parameter the standard value of $A/8$ MeV^{-1}, and compound-nucleus spin distributions were calculated taking into account the Bass nuclear potential [59]. Optical potential parameters for the evaporation of α's were introduced from the work of Huizenga and Igo [60] based on α scattering from very low energies to 50 MeV and 20 target nuclei with $10 \leqslant Z \leqslant 92$. The procedure is illustrated in Fig. 4, taking as an example the α spectra recorded in telescopes T1 and T2 at 22 MeV. The final simulations (sum of all four processes) for all three projectile energies are shown in Fig. 3.

The ^{3}He particles are produced via direct processes; that is, breakup and ^{4}He stripping. As already stated, breakup is predicted by preliminary CDCC calculations to contribute very little to the ^{3}He production and therefore this procedure was omitted from the simulations. In the same way as for the α-particle production, missing counts due to the telescope threshold (ΔE thickness) were estimated by comparing simulated with experimental spectra (Fig. 5).

After correcting for missing counts, the integrated ^{3}He and ^{4}He particle yields for each strip—that is, for

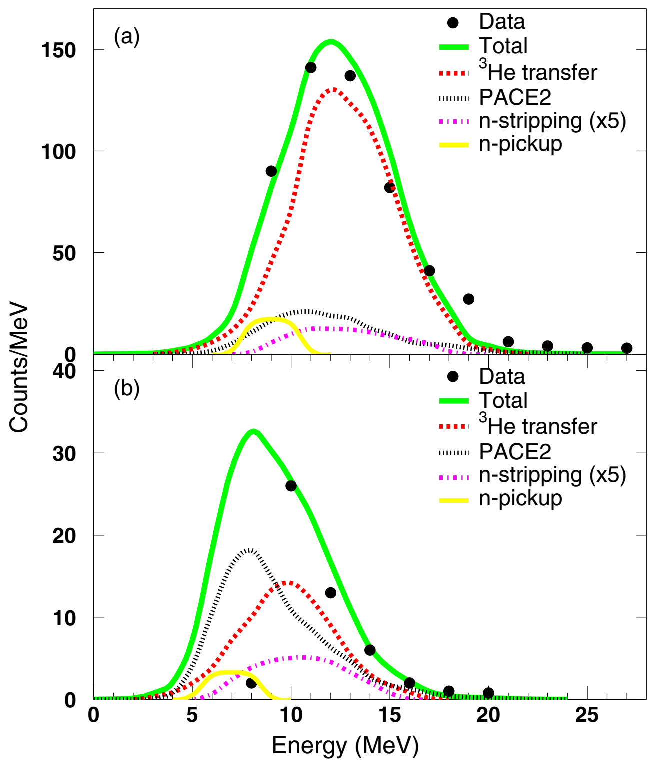

FIG. 4. Decomposition of the simulated alpha energy spectra at 22 MeV for telescopes (a) T1 and (b) T2 due to the compound-nucleus process (dotted black line) and direct processes as follows: the dot-dashed magenta line indicates the α spectrum due to neutron stripping, the solid yellow line that due to neutron pickup, and the dashed red line that due to ^{3}He transfer. The multiplication factors are arbitrary values for the purposes of presenting the various processes only.

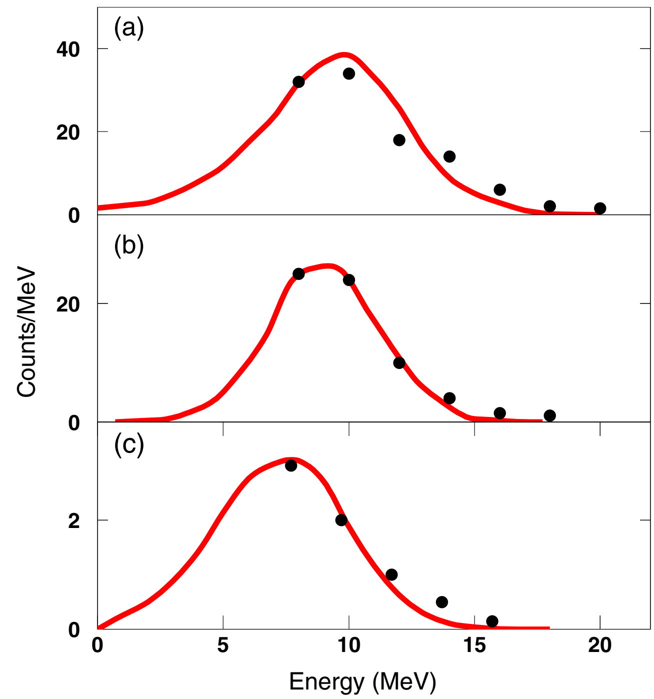

FIG. 5. ^{3}He energy spectra for telescope T1 (at 27°) for the three bombarding energies (a) 22 MeV, (b) 20 MeV, and (c) 13 MeV. The solid line is a simulated spectrum taking into account the α transfer.

particular angles—were transformed to cross sections taking into account the flux and target thickness deduced from a simultaneous elastic scattering measurement, to be presented elsewhere. Elastically scattered ^{7}Be particles were recorded simultaneously with the particle reaction products in our DSSSD detectors and in the most forward strips the scattering is Rutherford, allowing an accurate flux and target normalization. An elastic scattering measurement under the same conditions with a lead target ensured the correct determination of the solid angles.

III. DATA REDUCTION

Angular distributions for ^{3}He and ^{4}He particles were obtained under the experimental conditions described in the previous section, and are presented in Figs. 6 and 7, respectively. Each data point in these figures results from a weighted mean between three successive angles, to improve statistics. It is obvious from Fig. 6 that the ^{3}He-particle angular distribution is forward peaked at all three energies, pointing to direct mechanisms. On the other hand the ^{4}He-particle distributions, presented in Fig. 7, are forward peaked but are also extended with substantial cross sections at backward angles. This points to a more complex situation where both direct and compound mechanisms are present.

In more detail the only two mechanisms leading to ^{3}He-particle production are breakup and ^{4}He stripping.

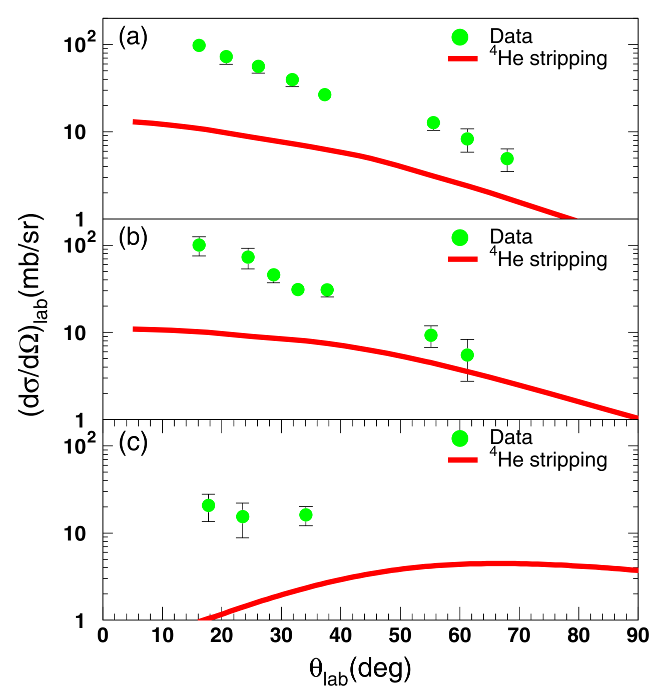

FIG. 6. Angular distributions for the ^{3}He-particle production. (a) 22 MeV, (b) 20 MeV, and (c) 13 MeV. Experimental points are denoted by the solid green circles, DWBA calculations for ^{4}He transfer by the solid red line.

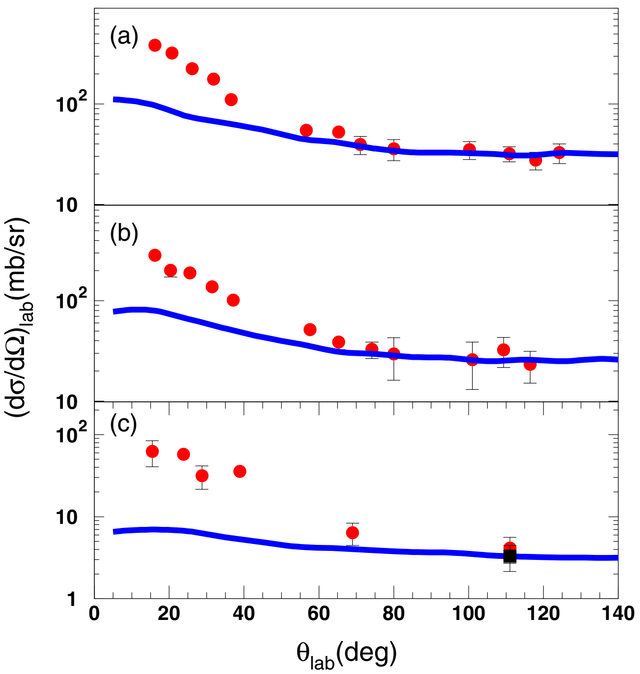

FIG. 7. Angular distributions for the ^{4}He-particle production (total cross sections) at (a) 22 MeV, (b) 20 MeV, and (c) 13 MeV. The solid line represents a calculation with the evaporation code PACE2 normalized to the backward angle data. For 13 MeV the black square represents the experimental datum minus the estimated contribution from direct processes, because in that case we expect a significant direct contribution.

Unfortunately, due to the low statistics and the geometrical efficiency of our detector setup, we did not record any coincidence events between ^{4}He and ^{3}He, the clear signature of an exclusive breakup event. Therefore, integrating the angular distributions we can give an inclusive cross section for both outgoing channels. The results are presented in Table I. However, estimating the breakup channel via preliminary CDCC calculations to be small, we can say that most of the inclusive cross sections are due to ^{4}He stripping, by which we denote a process whereby a ^{4}He cluster is transferred from the projectile to the target, although this need not be a "transfer reaction" in the usual sense. This is consistent with previous data concerning the ^{7}Be + ^{58}Ni system [33] and it seems to be a more general property of reactions involving weakly bound nuclei presenting a cluster structure. For example, in Ref. [21], where exclusive measurements are reported for ^{7}Li + ^{93}Nb, t stripping is suggested as the main direct mechanism of α production. The experimental angular distributions are compared in Fig. 6 with ^{4}He-transfer DWBA calculations, to be described in the following section. The calculated angular distributions (which were transformed into the laboratory frame) show less pronounced forward peaking than the measured ones as well as underpredicting the absolute magnitude.

For the ^{4}He-particle production many different mechanisms can contribute. These are the evaporation of α particles via the formation of a compound nucleus and direct mechanisms such as breakup ($S_\alpha = 1.586$ MeV), neutron stripping [^{7}Be + ^{28}Si → ^{6}Be(^{4}He + p + p) + ^{29}Si with $Q = -2.20$ MeV], neutron pickup [^{7}Be + ^{28}Si → ^{8}Be(^{4}He + ^{4}He) + ^{27}Si with $Q = 1.72$ MeV), and finally ^{3}He stripping (^{7}Be + ^{28}Si → ^{4}He + ^{31}S with $Q = 10.89$ MeV). To disentangle the compound-nucleus channel from the direct part we follow a standard technique as applied previously to the ^{6,7}Li + ^{28}Si systems [18,24,45]. We calculated the angular distributions of the evaporated alphas with the PACE2 code as described above, which were then renormalized to the data from the backward detectors T3 and T4. The procedure is illustrated in Fig. 7. For the lowest projectile energy of 13 MeV, due to the lower statistics data from the middle and backward detectors were summed over the whole detector and the differential cross sections obtained were assigned to the middle angle of each detector.

Angular distributions for the direct components are presented in Fig. 8. They were obtained by subtracting the compound-nucleus contributions from the total α production cross sections. DWBA predictions for neutron stripping (^{7}Be + ^{28}Si → ^{6}Be + ^{29}Si → ^{4}He + 2p + ^{29}Si) and neutron pickup (^{7}Be + ^{28}Si → ^{8}Be + ^{27}Si → ^{4}He + ^{4}He + ^{27}Si) are also shown on the same figure. The theoretical angular distributions, determined in the center-of-mass frame, were transformed to the laboratory frame using the same Monte Carlo program used in the spectrum simulations, and the resulting α-particle angular distributions obtained from the decay of the unbound ^{6}Be and ^{8}Be ejectiles are plotted. It can be seen that the production of α particles via these processes is small (note that the curves on the plot are multiplied by a factor of 2 in order better to show the two contributions on a reasonable scale). The remaining part should therefore be due to ^{3}He stripping, although this cannot be quantified by DWBA calculations due to the lack of appropriate spectroscopic factors in the literature. Again, by ^{3}He stripping we denote a process whereby a ^{3}He cluster is transferred from the projectile to the target which need not be a conventional "transfer reaction." As noted for the ^{3}He production, this seems to

TABLE I. ^{4}He- and ^{3}He-particle production cross sections. The second column gives the total cross section for ^{4}He-particle production. The third and fourth columns give cross sections for ^{4}He- and ^{3}He-particle production, respectively, due to direct mechanisms. Finally, the fifth column gives the total cross sections due to the direct channels, deduced as the sum of ^{4}He and ^{3}He cross sections.

E_{lab} (MeV)	$\sigma^{^4He}_{total}$ (mb)	$\sigma^{^4He}_{direct}$ (mb)	$\sigma^{^3He}_{direct}$ (mb)	σ direct (mb)
22	763 ± 69	252 ± 111	114 ± 17	366 ± 112
20	653 ± 72	234 ± 127	101 ± 19	335 ± 128
13	131 ± 26	81 ± 32	30 ± 8	111 ± 33

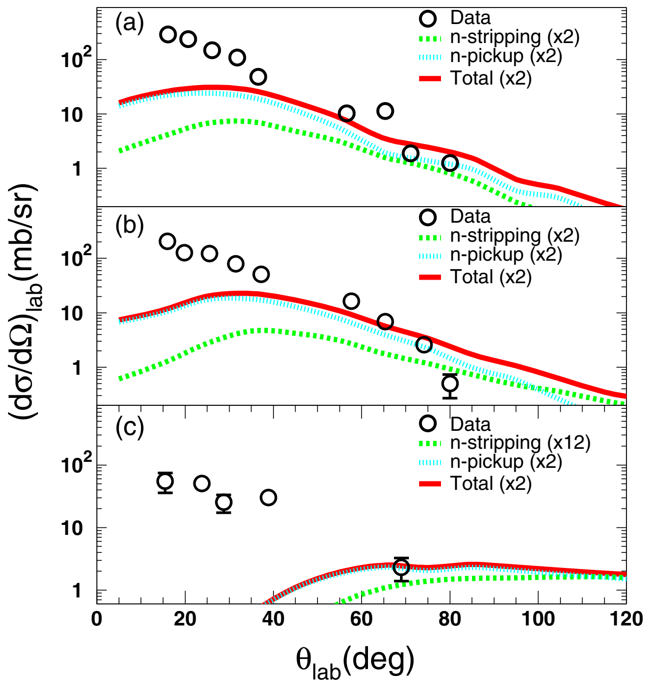

FIG. 8. Angular distributions for ^{4}He-particle production due to direct mechanisms at (a) 22 MeV, (b) 20 MeV, and (c) 13 MeV. The data are denoted by the open circles, DWBA for neutron stripping by the dashed green line and for neutron pickup by the dotted cyan line. The sum of the two processes is denoted by the solid red line. The remainder may be attributed to ^{3}He stripping. The multiplication factors are arbitrary for the purposes of displaying the various processes only. Errors are due solely to the experimental uncertainties of total α production.

be common ground supported by other inclusive as well as exclusive measurements [21,33].

The total (experimental α-particle angular distributions) and compound-nucleus (theoretical α-particle angular distributions renormalized to the backward-angle experimental data) angular distributions were integrated over angle, and the direct (total − compound) and compound-nucleus α-particle production cross sections thus obtained are included in Tables I and II. Errors were assigned by taking into account the best fits and a reduced χ^2-plus-1 analysis ($\chi^2/N + 1$). In Table II we also present the total fusion cross sections, obtained by making use of the evaporated α-particle multiplicities calculated in our statistical model approach. It should be noted however that the

TABLE III. α-particle multiplicities obtained with the code PACE2 and using three different optical model parameters. In the second column appear multiplicities with the Huizenga and Igo optical parameters [60], $M1$, third column with the McFadden and Satchler optical parameters [62], $M2$, fourth column with the Satchler optical parameters [63], $M3$, and finally in the fifth column appear the mean of these multiplicities, M_{mean}, and standard deviation.

Energy (MeV)	$M1$	$M2$	$M3$	M_{mean}
22	0.63	0.55	0.58	0.59 ± 0.04
20	0.57	0.50	0.52	0.53 ± 0.04
13	0.37	0.31	0.34	0.34 ± 0.03

determination of fusion cross sections may be liable to possible shortcomings of the statistical model code. A comprehensive analysis of ^{8}B fusion data in different compound-nucleus models in Ref. [61] highlighted this problem. Our case is slightly different from the point of view that we possess α-particle angular distributions. In this respect the parameter introduced into our compound-nucleus code—that is, the total fusion cross section—does not affect our results as the theoretical angular distributions are renormalized to the backward angle data. However, the level density and the optical potential parameters for the evaporation of α's, which are used to extract fusion from the α-particle production can introduce uncertainties in the fusion itself via the calculated multiplicities. Different level densities varying by, e.g., $\sim$6% ($A/7.5$ or $A/8.5$) produce multiplicities larger or smaller by approximately 1% to 2% introducing negligible error to the fusion. Taking into account, however, that the optical model parameters for α particle emission can affect strongly these quantities and therefore fusion, we have estimated such an uncertainty of the multiplicities by taking into account, for the Huizenga and Igo optical parameters, those of McFadden and Satchler [62] and Satchler [63]. The last two are based in the analysis of 24.7 and 28 MeV α particles scattered by various targets with atomic numbers, $8 \leqslant Z \leqslant 92$ and $10 \leqslant Z \leqslant 50$ respectively. The obtained multiplicities are given in Table III together with a mean and a standard deviation, which is used for the extraction of fusion cross sections and their uncertainty.

Finally, total reaction cross sections were deduced by summing the fusion cross sections and the ^{3,4}He-particle cross sections due to direct reaction mechanisms. The results are given in the fifth column of Table II and are found to be in very good agreement with total reaction cross sections, given in column 6, obtained previously [34], according to

TABLE II. Details of our results for the compound channel. The second column gives cross sections for ^{4}He-particle production due to the compound mechanism. The third column gives the multiplicity of the evaporated α's, calculated with the PACE2 code [58]. The fourth column gives the extracted total fusion cross sections and the fifth column the total reaction cross sections obtained by summing the fusion cross sections and the direct cross sections (the fourth column of this table and the fifth column of Table I. Last, in the sixth column we give total reaction cross sections, σ_p, according to the prediction described for light targets in Ref. [34]

E_{lab} (MeV)	$\sigma^{^4\text{He}}_{\text{compound}}$ (mb)	α multiplicity	σ fusion (mb)	σ total (mb)	σ_p (mb)
22	511 ± 87	0.59 ± 0.04	866 ± 159	1232 ± 195	1118
20	419 ± 105	0.53 ± 0.04	791 ± 205	1126 ± 242	990
13	50 ± 18	0.34 ± 0.03	147 ± 54	258 ± 63	347

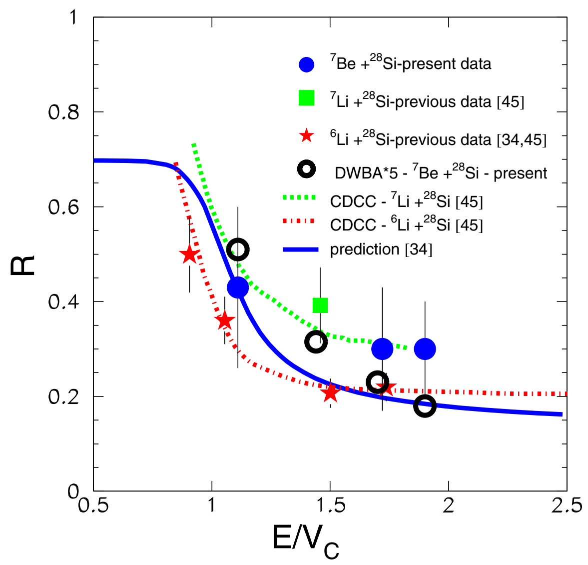

FIG. 9. Energy evolution of the ratios, R, of direct to total reaction cross section. The present results for $^7\mathrm{Be} + {}^{28}\mathrm{Si}$, denoted by the solid blue circles, are compared with previous results for $^6\mathrm{Li} + {}^{28}\mathrm{Si}$ (solid red stars) and $^7\mathrm{Li} + {}^{28}\mathrm{Si}$ (green square). They are also compared with a phenomenological prediction (solid blue line) for $^7\mathrm{Be} + {}^{28}\mathrm{Si}$, outlined in Ref. [34]. Previous calculated ratios for $^6\mathrm{Li} + {}^{28}\mathrm{Si}$ and $^7\mathrm{Li} + {}^{28}\mathrm{Si}$ are also shown as the dot-dashed red line and dotted green line, respectively [45]. These calculations were based on total reaction cross sections deduced from a CDCC calculation and fusion cross sections deduced from a BPM model. In the latter case an energy dependent potential was taken into account, derived from the CDCC calculations according to the prescription of Thompson [82]. The open circles correspond to the present DWBA calculations, multiplied by 5 to match the data.

a global prediction for light targets. Having obtained direct and total reaction cross sections, we then formed the ratios of direct to total reaction cross section, R = direct/total. The present ratios are compared in Fig. 9 with previous results for $^{6,7}\mathrm{Li} + {}^{28}\mathrm{Si}$ [34]. The trend of the energy evolution for all three projectiles is the same; that is, approaching the barrier from higher to lower energies the direct contribution rises. On the other hand it is obvious that the ^{7}Be results follow in magnitude the results for ^{7}Li rather than those for ^{6}Li. This indicates a larger contribution from direct processes for the two mirror nuclei than for ^{6}Li, which we will see in what follows acts at the expense of the fusion cross sections. The prediction of Ref. [34] is in good qualitative agreement but only fair quantitative agreement with experiment. This prediction was calculated for $^7\mathrm{Be} + {}^{28}\mathrm{Si}$ but similar results can be produced for the other two systems. In the same figure we also present ratios as deduced from our DWBA calculations. As was already seen, the calculated transfer cross sections are significantly lower than the measured values. Therefore, these values, while they describe roughly the shape of the energy dependence of the ratios of direct to total reaction cross section, at least at the lower energies, fail to give quantitative agreement. It should be noted that the theoretical R values plotted on Fig. 9 were multiplied by a factor of ∼5 to match the data at the lower energies.

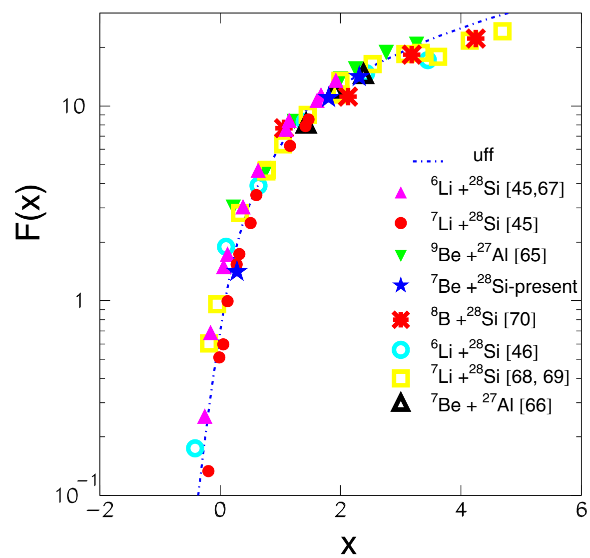

FIG. 10. Reduced fusion cross sections for various stable and radioactive projectiles incident on ^{28}Si and ^{27}Al targets as a function of the parameter x (reduced energy). The reduction was made according to Ref. [64]. The line represents the universal fusion function, uff, according to the same prescription [64].

The fusion cross sections, displayed in Table II, are reduced according to Ref. [64] in a fusion-function context and are compared in Fig. 10 with previously measured fusion cross sections for ^{9}Be [65], ^{7}Be [66], ^{6,7}Li [45,46,67–69], and ^{8}B [70] on the same or similar mass targets (^{27}Al and ^{28}Si). In more detail, the reduction of the data follows a scheme where the fusion cross section, σ_F, and the energy, $E_\mathrm{c.m}$, of the projectile can be reduced to fusion functions, $F(x)$, and the quantity x, respectively, according to the formulas

$$\sigma_\mathrm{F} \rightarrow F(x) = \frac{2E_\mathrm{c.m.}}{\hbar\omega R_\mathrm{C}}\sigma_\mathrm{F} \qquad (1)$$

and

$$E_\mathrm{c.m.} \rightarrow x = \frac{E_\mathrm{c.m.} - V_\mathrm{C}}{\hbar\omega}. \qquad (2)$$

Fusion functions, $F(x)$, were determined as a function of x for all data via the above relations. Curvatures ($\hbar\omega$), radii (R_C), and potential heights (V_C) were deduced using the Christensen-Winther potential [71] and the obtained values are included in Table IV.

TABLE IV. Potential height, radius and curvature for various systems considered in this work, calculated using the Christensen-Winther potential [71]

Reaction	V_C (MeV)	R_C (fm)	$\hbar\omega$ (MeV)
$^8\mathrm{B} + {}^{28}\mathrm{Si}$	11.67	7.935	3.662
$^6\mathrm{Li} + {}^{28}\mathrm{Si}$	7.008	7.932	3.223
$^7\mathrm{Li} + {}^{28}\mathrm{Si}$	6.840	8.145	2.968
$^7\mathrm{Be} + {}^{28}\mathrm{Si}$	9.351	7.922	3.478
$^7\mathrm{Be} + {}^{27}\mathrm{Al}$	8.681	7.925	3.371
$^9\mathrm{Be} + {}^{27}\mathrm{Al}$	8.358	8.269	2.955

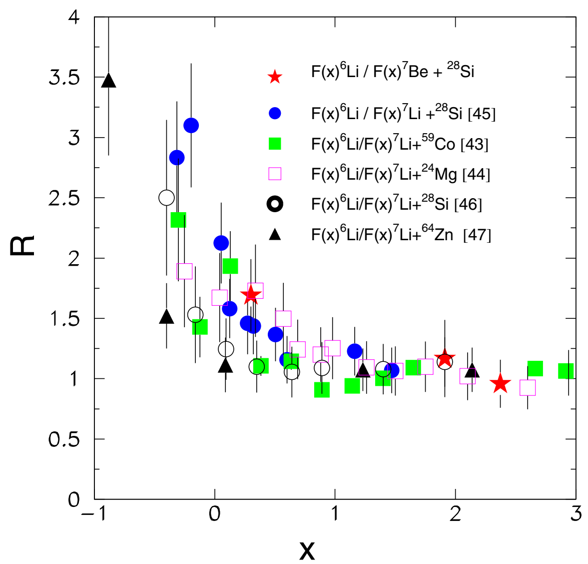

FIG. 11. Ratios of fusion functions for ^{6}Li + ^{28}Si versus ^{7}Li + ^{28}Si compared with ratios of fusion functions for ^{6}Li + ^{28}Si versus ^{7}Be + ^{28}Si as a function of the parameter x (reduced energy). Other ratios for various targets of ^{6}Li versus ^{7}Li are also included.

The present and previous data follow the same trend as the universal fusion function (uff), defined in Ref. [64] as

$$F_0(x) = \ln[1 + \exp(2\pi x)], \tag{3}$$

and show good consistency between each other and with the uff to within an uncertainty band of 10% to 20%. In principle variations between the data and the uff are expected below the barrier due to channel coupling effects. However, to link any such variations with significance to a particular coupling scheme the assigned errors should be small, which is not the case here. Nevertheless, we may attempt to map variations between the cross sections obtained for ^{6}Li and ^{7}Li and those for ^{7}Be, seeking similarities between ^{7}Be and ^{6}Li or ^{7}Li. Comparisons of previously measured fusion cross sections for ^{6}Li + ^{28}Si and ^{7}Li + ^{28}Si [45] with the present results for ^{7}Be + ^{28}Si by forming ratios of the fusion functions for ^{6}Li to those for ^{7}Li and ^{7}Be are presented in Fig. 11. It is seen that hindrance of the fusion cross sections for ^{7}Li with respect to those for ^{6}Li starts near the barrier (already at $\sim E = 1.1 V_C$, $R = 1.5$) and becomes significant well below the barrier to the extent of 70%. The same trend is seen for the present data for ^{7}Be, indicating similarity between ^{7}Be and ^{7}Li rather than ^{6}Li as theory had predicted for the elastic scattering [72]. It should be noted, however, that in Ref. [72] calculations were performed for elastic scattering of ^{6,7}Li and ^{7}Be on a ^{208}Pb target taking into account breakup coupling to the continuum. For this heavy target, breakup could play a critical role. Further, an inspection of Figs. 9 and 11 indicates that the hindrance of ^{7}Li fusion and perhaps of ^{7}Be compared to ^{6}Li may be attributed to large transfer channels which become more significant than fusion as the barrier is approached from higher to lower energies and are larger for ^{7}Li and ^{7}Be than for ^{6}Li. It should be underlined, however, that for ^{7}Be more measurements well below the barrier are needed in order to come to firm conclusions.

IV. THEORETICAL CALCULATIONS: DWBA

DWBA calculations were required for the following reactions that ultimately lead to ^{4}He as one of the outgoing particles: ^{28}Si(^{7}Be, ^{6}Be)^{29}Si, ^{28}Si(^{7}Be, ^{8}Be)^{27}Si, and ^{28}Si(^{7}Be, ^{4}He)^{31}S. Calculations were also needed for the ^{28}Si(^{7}Be, ^{3}He)^{32}S reaction, producing ^{3}He particles. All calculations used the global ^{7}Li optical model parameters of Ref. [73] as a surrogate for the entrance channel ^{7}Be + ^{28}Si potentials. For the rest of the details we take the different reactions in turn, beginning with the ^{28}Si(^{7}Be, ^{6}Be)^{29}Si 1n stripping.

Since ^{6}Be is particle unstable there are no optical potentials available for systems involving this nucleus, and the global ^{6}Li parameters of Ref. [73] were used instead. Stripping to both the 0^{+} ground state and 1.67 MeV 2^{+} resonances of ^{6}Be was included, the spectroscopic factors for the $\langle ^{7}\mathrm{Be} \mid ^{6}\mathrm{Be} + n\rangle$ overlaps being taken from Ref. [74]. The stripped neutron was bound to the ^{6}Be core in a Woods-Saxon well of radius $1.25 \times A^{1/3}$ fm and diffuseness 0.65 fm. A Thomas-form spin-orbit potential of the same geometry and fixed depth of 6.0 MeV was also included, the depth of the central well being adjusted to give the experimental binding energy. Stripping to the following states in ^{29}Si was included: 0.0 MeV $1/2^{+}$, 1.27 MeV $3/2^{+}$, 2.03 MeV $5/2^{+}$, 3.62 MeV $7/2^{-}$, 4.94 MeV $3/2^{-}$, and 6.20 MeV $7/2^{-}$, the $\langle ^{29}\mathrm{Si} \mid ^{28}\mathrm{Si} + n\rangle$ overlaps being taken from Ref. [75].

For the ^{28}Si(^{7}Be, ^{8}Be)^{27}Si 1n-pickup reaction, ^{8}Be also being particle unstable, the global ^{7}Li optical potential parameters of Ref. [73] were used in the exit channel. Pickup to both the 0^{+} ground state and 3.03 MeV 2^{+} resonances of ^{8}Be was included, the spectroscopic factors for the $\langle ^{8}\mathrm{Be} \mid ^{7}\mathrm{Be} + n\rangle$ overlaps being taken from Ref. [74]. The picked-up neutron was bound to the ^{7}Be core in a Woods-Saxon well of radius $1.25 \times A^{1/3}$ fm and diffuseness 0.65 fm. A Thomas-form spin-orbit potential of the same geometry and fixed depth of 6.0 MeV was also included, the depth of the central well being adjusted to give the experimental binding energy. Pickup leading to the following states in ^{27}Si was included: 0.0 MeV $5/2^{+}$, 0.78 MeV $1/2^{+}$, and 0.96 MeV $3/2^{+}$, the $\langle ^{28}\mathrm{Si} \mid ^{27}\mathrm{Si} + n\rangle$ overlaps being taken from Ref. [76]. Of course, in this reaction the ^{8}Be ejectile spontaneously decays to give two outgoing α particles. This was taken into account in producing the curves plotted on Fig. 8.

Calculations for the ^{28}Si(^{7}Be, ^{4}He)^{31}S ^{3}He-stripping reaction are more problematic since there are no suitable spectroscopic factors available in the literature for the $\langle ^{31}\mathrm{S} \mid ^{28}\mathrm{Si} + n\rangle$ overlaps. The only experimental indication of which states in ^{31}S might be populated comes from a measurement of the ^{28}Si(^{6}Li, ^{3}H)^{31}S reaction [77] in which the 0.0 MeV $1/2^{+}$, 1.25 MeV $3/2^{+}$, and 4.45 MeV $7/2^{-}$ states were the main states in ^{31}S observed (no angular distributions were measured but a spectrum is given). However, the Q-matching conditions for the ^{28}Si(^{7}Be, ^{4}He)^{31}S reaction favor population of highly excited states ($E_{\mathrm{ex}} > 10$ MeV) close to or above the ^{3}He emission threshold. Such calculations were therefore not attempted since there is insufficient information available to yield meaningful results.

Finally, for the ^{28}Si(^{7}Be,^{3}He)^{32}S ^{4}He-stripping reaction the global ^{3}He optical model parameters of Ref. [78] were used in the exit channel. The spectroscopic factor for the $\langle ^7\mathrm{Be} \mid ^4\mathrm{He} + ^3\mathrm{He}\rangle$ overlap was set equal to 1.0 and the ^{4}He + ^{3}He binding potential was taken from Ref. [79]. Stripping to the following states in ^{32}S was included: 0.0 MeV 0^+, 2.23 MeV 2^+, 3.78 MeV 0^+, 4.46 MeV 4^+, 5.01 MeV 3^-, 5.80 MeV 1^-, 6.76 MeV 3^-, 7.43 MeV 1^-, and 8.49 MeV 1^-. The final two states being unbound with respect to the ^{4}He emission threshold of ^{32}S, the form factors for these states were calculated using the weak binding energy approximation with a "binding energy" of 0.01 MeV. Spectroscopic factors were the ^{28}Si(^{6}Li,d)^{32}S values of Ref. [80].

V. SUMMARY AND CONCLUSIONS

We have investigated the reaction mechanisms for the ^{7}Be + ^{28}Si system at near-barrier energies ($\sim 1.1 \times V_C$ to $\sim 2 \times V_C$) by detecting the light particles ^{3}He and ^{4}He, the cluster constituents of ^{7}Be. Angular distributions of the light particles were measured at three bombarding energies: 13, 20, and 22 MeV. According to the measured light-particle production and our calculations of relevant compound-nucleus and direct reaction processes, large ^{3}He- and ^{4}He-stripping channels may be inferred: Our DWBA calculations of single neutron stripping and pickup should be reasonably quantitatively accurate since such processes are usually well described. Even an uncertainty as large as a factor of 2 in the absolute values does not affect our conclusion that these processes are unable to describe the bulk of the direct part of the ^{4}He production cross section. The same comment applies to our preliminary CDCC calculations with respect to the breakup contributions. In this context, by "stripping" we denote a process whereby a ^{3}He or ^{4}He cluster is transferred from the projectile to the target, although the mechanism may not be that of a conventional transfer reaction. An incomplete fusion process would lead to the same end result and this possibility has also been discussed in the literature; see, e.g., Refs. [47,81]. At present it is not possible to distinguish between these possibilities—conventional cluster transfer and incomplete fusion—at least experimentally. Indeed, incomplete fusion defined as a breakup event followed by fusion of one of the fragments might plausibly be alternatively modeled as a "two-step transfer" event, with the weakly bound projectile "inelastically excited" to the (nonresonant) continuum followed by cluster transfer. A two-step transfer picture would also allow inclusion of resonant breakup (at least in principle) which will not contribute to incomplete fusion due to the lifetimes of the resonant states; see, e.g., Ref. [81].

Calculations of conventional ^{3}He and ^{4}He cluster transfer which might shed more light on this question are problematical. The optimum Q values for these processes vary from about -4 to -8 MeV for the ^{28}Si(^{7}Be,^{4}He)^{31}S reaction and from about -4 to about -9 MeV for the ^{28}Si(^{7}Be,^{3}He)^{32}S reaction for incident energies of 13 and 22 MeV, respectively. This implies preferential population of states in the residual nucleus at excitation energies where no spectroscopic factors are available (indeed there are no spectroscopic factors available at all for the $\langle ^{31}\mathrm{S} \mid ^{28}\mathrm{Si} + ^3\mathrm{He}\rangle$ overlap). DWBA calculations were performed for the ^{28}Si(^{7}Be,^{3}He)^{32}S reaction using available spectroscopic factors but these stopped short of states covering the excitation energy range in ^{32}S covered by the optimum Q value. This, coupled with the fact that *absolute* spectroscopic factors for α transfers are notoriously ill defined—factors of 5 or more between values for the same target obtained with different reactions and at different bombarding energies being common—may easily explain why, although the DWBA calculations are in reasonable qualitative agreement with the data, for a quantitative agreement the theoretical cross sections have to be multiplied by a factor of about 5. The shapes of the measured angular distributions are somewhat more forward peaked than the calculated ones, which may indicate a more complicated reaction mechanism than the one-step transfer assumed in the DWBA. However, since the DWBA calculations do not cover the range in ^{32}S excitation energies spanning the optimum Q value and given the uncertainties in the input (entrance and exit channel optical potentials, for example) it remains an open question whether the ^{3}He-particle production can be adequately modeled as a conventional α-particle transfer reaction.

For the α-particle angular distributions the compound contribution was modeled by calculations carried out in a statistical model framework enabling the direct component to be separated. Both the fusion cross sections and ratios of direct to total reaction cross sections were then deduced. The present energy evolution of direct versus compound-nucleus mechanisms exhibits the same increasing behavior approaching the barrier from higher to lower energies as for the stable weakly bound projectiles ^{6}Li and ^{7}Li. The results are quantitatively closer to those for ^{7}Li, where we observe larger direct to total ratios due to an enhancement of transfer channels at the expense of fusion. Indeed, the present fusion results for ^{7}Be, if compared with those for ^{6,7}Li on the same target, ^{28}Si, are in perfect agreement with previous results for ^{7}Li, indicating a possible similarity of ^{7}Be to ^{7}Li. Phenomenological support for this suggestion is also given by the resemblance in shape of the α angular distributions for ^{7}Be with those for ^{7}Li rather than the ^{6}Li ones.

With regard to fusion itself, for the energy range under investigation here, 1.1 to $2 \times V_C$ and within the constraints of the compound-nucleus model employed, the cross sections closely follow the uff curve—that is, a single barrier penetration calculation—to within an uncertainty of $\sim\pm 10\%$. This does not preclude the behavior observed below the barrier for the same projectile but heavier targets where small to very large enhancements have been reported. It is therefore an open question whether fusion below the barrier for proton rich nuclei is enhanced, in contrast to the behavior of neutron rich nuclei, and whether this is connected with the target mass. It should be underlined, however, that the present results, considered in a systematic framework with the low mass target ^{28}Si, indicate a hindrance of fusion below the barrier rather than an enhancement.

In summary, the ^{3}He and ^{4}He production cross sections for the ^{7}Be + ^{28}Si system have been measured at three near-barrier incident energies. Our analysis indicates that the main production processes are ^{4}He stripping and ^{3}He stripping, respectively, although we are not at present able to distinguish the exact reaction mechanism; standard transfer reactions or a partial fusion mechanism are both possible and plausible candidates. Fusion cross sections were inferred from the ^{4}He cross sections by means of statistical model calculations. To within the uncertainties that this method involves these cross sections follow the uff curve and are consistent with a single barrier penetration calculation. The behavior as a function of energy of the direct to total reaction cross section ratios for ^{7}Be + ^{28}Si more closely follow the trend of those for ^{7}Li + ^{28}Si, pointing to a greater importance of transfer reactions for these two mirror nuclei at near-barrier energies compared to ^{6}Li.

ACKNOWLEDGMENT

The research leading to these results was partially funded by the European Union Seventh Framework Programme FP7/2007-2013 under Grant Agreement No. 262010-ENSAR.

[1] L. F. Canto, P. R. S. Gomes, R. Donangelo, and M. S. Hussein, Phys. Rep. **424**, 1 (2006).
[2] N. Keeley, N. Alamanos, K. W. Kemper, and K. Rusek, Prog. Part. Nucl. Phys. **63**, 396 (2009).
[3] N. Keeley, R. Raabe, N. Alamanos, and J. L. Sida, Prog. Part. Nucl. Phys. **59**, 579 (2007).
[4] P. R. S. Gomes, J. Lubian, L. F. Canto, D. R. Otomar, D. R. Mendes, Jr., P. N. de Faria, R. Linares, L. Sigaud, J. Rangel, J. L. Ferreira, E. Ferioli, B. Paes, E. N. Cardozo, M. R. Cortes, M. J. Ermamatov, P. Lotti, and M. S. Hussein, Few-Body Syst. **57**, 165 (2016)
[5] C. Beck, N. Rowley, P. Papka, S. Courtin, M. Rousseau, F. A. Souza, N. Carlin, R. Liguori Neto, M. M. de Moura, M. G. Del Santo, A. A. P. Suaide, M. G. Munhoz, E. M. Szanto, A. Szanto de Toledo, N. Keeley, A. Diaz-Torres, and K. Hagino, Nucl. Phys. A **834**, 440c (2010).
[6] C. Beck, Nucl. Phys. A **787**, 251c (2007).
[7] J. J. Kolata, V. Guimaraes, and E. F. Aguilera, Eur. Phys. J **A 52**, 123 (2016).
[8] L. F. Canto, P. R. S. Gomes, R. Donangelo, J. Lubian, and M. S. Hussein, Phys. Rep. **596**, 1 (2015)
[9] B. B. Back, H. Esbensen, C. L. Jiang, and K. E. Rehm, Rev. Mod. Phys. **86**, 317 (2014)
[10] A. Pakou, N. Alamanos, N. M. Clarke, N. J. Davis, G. Doukelis, G. Kalyva, M. Kokkoris, A. Lagoyannis, T. J. Mertzimekis, A. Musumarra, N. G. Nicolis, C. Papachristodoulou, N. Patronis, G. Perdikakis, D. Pierroutsakou, D. Roubos, K. Rusek, S. Spyrou, and Ch. Zarkadas, Phys. Lett. B **633**, 691 (2006).
[11] F. A. Souza, C. Beck, N. Carlin, N. Keeley, R. Liguori Neto, M. M. de Moura, M. G. Munhoz, M. G. Del Santo, A. A. P. Suaide, E. M. Szanto, and A. Szanto de Toledo, Nucl. Phys. A **821**, 36 (2009).
[12] F. A. Souza, N. Carlin, C. Beck, N. Keeley, A. Diaz-Torres, R. Liguori Neto, C. Siqueira-Mello, M. M.de Moura, M. G. Munhoz, R. A. N. Oliveira, M. G. Del Santo, A. A. P. Suaide, E. M. Szanto, and A. Szanto de Toledo, Eur. Phys. J. A **44**, 181 (2010).
[13] F. A. Souza, N. Carlin, C. Beck, N. Keeley, A. Diaz-Torres, R. Liguori Neto, C. Siqueira-Mello, M. M.de Moura, M. G. Munhoz, R. A. N. Oliveira, M. G. Del Santo, A. A. P. Suaide, E. M. Szanto, and A. Szanto de Toledo, Nucl. Phys. A **834**, 420c (2010).
[14] C. Signorini, A. Edifizi, M. Mazzocco, M. Lunardon, D. Fabris, A. Vitturi, P. Scopel, F. Soramel, L. Stroe, G. Prete, E. Fioretto, M. Cinausero, M. Trotta, A. Brondi, R. Moro, G. La Rana, E. Vardaci, A. Ordine, G. Inglima, M. La Commara, D. Pierroutsakou, M. Romoli, M. Sandoli, A. Diaz-Torres, I. J. Thompson, and Z. H. Liu, Phys. Rev. C **67**, 044607 (2003).
[15] D. H. Luong, M. Dasgupta, D. J. Hinde, R. du Rietz, R. Rafiei, C. J. Lin, M. Evers, and A. Diaz-Torres, Phys. Rev. C **88**, 034609 (2013).
[16] S. Santra, V. V. Parkar, K. Ramachandran, U. K. Pal, A. Shrivastava, B. J. Roy, B. K. Nayak, A. Chatterjee, R. K. Choudhury, and S. Kailas, Phys. Lett. B **677**, 139 (2009).
[17] J. J. Kolata, H. Amro, F. D. Becchetti, J. A. Brown, P. A. DeYoung, M. Hencheck, J. D. Hinnefeld, G. F. Peaslee, A. L. Fritsch, C. Hall, U. Khadka, Patrick J. Mears, P. O'Rourke, D. Padilla, J. Rieth, Tabatha Spencer, and T. Williams, Phys. Rev. C **75**, 031302(R) (2007).
[18] A. Pakou, K. Rusek, N. Alamanos, X. Aslanoglou, S. Harissopulos, M. Kokkoris, A. Lagoyannis, T. J. Mertzimekis, A. Musumarra, N. G. Nicolis, C. Papachristodoulou, D. Pierroutsakou, and D. Roubos, Phys. Rev. C **76**, 054601 (2007).
[19] D. Gupta, C. Samanta, R. Kanungo, M. K. Sharan, S. Kailas, A. Chatterjee, K. Mahata, and A. Shrivastava, Nucl. Phys. A **646**, 161 (1999).
[20] A. Shrivastava, A. Navin, N. Keeley, K. Mahata, K. Ramachandran, V. Nanal, V. V. Parkar, A. Chatterjee, and S. Kailas, Phys. Lett. **B633**, 463 (2006).
[21] S. K. Pandit, A. Shrivastava, K. Mahata, N. Keeley, V. V. Parkar, P. C. Rout, K. Ramachandran, I. Martel, C. S. Palshetkar, A. Kumar, A. Chatterjee, and S. Kailas, Phys. Rev. C **93**, 061602(R) (2016).
[22] D. Gupta, C. Samanta, A. Chatterjee, S. Kailas, B. J. Roy, K. Mahata, and A. Shrivastava, Nucl. Phys. A **683**, 3 (2001).
[23] A. Pakou, N. Alamanos, A. Gillibert, M. Kokkoris, S. Kossionides, A. Lagoyannis, N. G. Nicolis, C. Papachristodoulou, D. Patiris, D. Pierroutsakou, E. C. Pollacco, and K. Rusek, Phys. Rev. Lett. **90**, 202701 (2003).
[24] A. Pakou, N. G. Nicolis, K. Rusek, N. Alamanos, G. Doukelis, A. Gillibert, G. Kalyva, M. Kokkoris, A. Lagoyannis, A. Musumarra, C. Papachristodoulou, G. Perdikakis, D. Pierroutsakou, E. C. Pollacco, A. Spyrou, and Ch. Zarkadas, Phys. Rev. C **71**, 064602 (2005).
[25] H. Kumawat, V. Jha, V. V. Parkar, B. J. Roy, S. Santra, V. Kumar, D. Dutta, P. Shukla, L. M. Pant, A. K. Mohanty, R. K. Choudhury, and S. Kailas, Phys. Rev. C **81**, 054601 (2010).
[26] C. S. Palshetkar, S. Santra, A. Shrivastava, A. Chatterjee, S. K. Pandit, K. Ramachandran, V. V. Parkar, V. Nanal, V. Jha, B. J. Roy, and S. Kailas, Phys. Rev. C **89**, 064610 (2014).
[27] V. Scuderi, A. Di Pietro, P. Figuera, M. Fisichella, F. Amorini, C. Angulo, G. Cardella, E. Casarejos, M. Lattuada, M. Milin, A. Musumarra, M. Papa, M. G. Pellegriti, R. Raabe, F. Rizzo, N. Skukan, D. Torresi, and M. Zadro, Phys. Rev. C **84**, 064604 (2011).

[28] A. Di Pietro, P. Figuera, F. Amorini, C. Angulo, G. Cardella, S. Cherubini, T. Davinson, D. Leanza, J. Lu, H. Mahmud, M. Milin, A. Musumarra, A. Ninane, M. Papa, M. G. Pellegriti, R. Raabe, F. Rizzo, C. Ruiz, A. C. Shotter, N. Soic, S. Tudisco, and L. Weissman, Phys. Rev. C **69**, 044613 (2004).
[29] E. F. Aguilera, J. J. Kolata, F. M. Nunes, F. D. Becchetti, P. A. DeYoung, M. Goupell, V. Guimaraes, B. Hughey, M. Y. Lee, D. Lizcano, E. Martinez-Quiroz, A. Nowlin, T. W. O'Donnell, G. F. Peaslee, D. Peterson, P. Santi, and R. White-Stevens, Phys. Rev. Lett. **84**, 5058 (2000).
[30] D. Escrig, A. M. Sanchez-Benitez, A. M. Moro, M. A. G. Alvarez, M. V. Andres, C. Angulo, M. J. G. Borge, J. Cabrera, S. Cherubini, P. Demaret, J. M. Espino, P. Figuera, M. Freer, J. E. Garcia-Ramos, J. Gomez-Camacho, M. Gulino, O. R. Kakuee, I. Martel, C. Metelko, F. Perez-Bernal, J. Rahighi, K. Rusek, D. Smirnov, O. Tengblad, and V. Ziman, Nucl. Phys. A **792**, 2 (2007).
[31] L. Acosta, A. M. Sanchez-Benitez, M. E. Gomez, I. Martel, F. Perez-Bernal, F. Pizarro, J. Rodriguez-Quintero, K. Rusek, M. A. G. Alvarez, M. V. Andres, J. M. Espino, J. P. Fernandez-Garcia, J. Gomez-Camacho, A. M. Moro, C. Angulo, J. Cabrera, E. Casarejos, P. Demaret, M. J. G. Borge, D. Escrig, O. Tengblad, S. Cherubini, P. Figuera, M. Gulino, M. Freer, C. Metelko, V. Ziman, R. Raabe, I. Mukha, D. Smirnov, O. R. Kakuee, and J. Rahighi, Phys. Rev. C **84**, 044604 (2011).
[32] A. Di Pietro, V. Scuderi, A. M. Moro, L. Acosta, F. Amorini, M. J. G. Borge, P. Figuera, M. Fisichella, L. M. Fraile, J. Gomez-Camacho, H. Jeppesen, M. Lattuada, I. Martel, M. Milin, A. Musumarra, M. Papa, M. G. Pellegriti, F. Perez-Bernal, R. Raabe, G. Randisi, F. Rizzo, G. Scalia, O. Tengblad, D. Torresi, A. M. Vidal, D. Voulot, F. Wenander, and M. Zadro, Phys. Rev. C **85**, 054607 (2012).
[33] M. Mazzocco, D. Torresi, D. Pierroutsakou, N. Keeley, L. Acosta, A. Boiano, C. Boiano, T. Glodariu, A. Guglielmetti, M. La Commara, J. A. Lay, I. Martel, C. Mazzocchi, P. Molini, C. Parascandolo, A. Pakou, V. V. Parkar, M. Romoli, K. Rusek, A. M. Sánchez-Benitez, M. Sandoli, O. Sgouros, C. Signorini, R. Silvestri, F. Soramel, V. Soukeras, E. Stiliaris, E. Strano, L. Stroe, and K. Zerva, Phys. Rev. C **92**, 024615 (2015).
[34] A. Pakou, D. Pierroutsakou, M. Mazzocco, L. Acosta, X. Aslanoglou, A. Boiano, C. Boiano, D. Carbone, M. Cavallaro, J. Grebosz, N. Keeley, M. La Commara, C. Manea, G. Marquinez-Duran, I. Martel, C. Parascandolo, K. Rusek, A. M. Sanchez-Benitez, O. Sgouros, C. Signorini, F. Soramel, V. Soukeras, E. Stiliaris, E. Strano, D. Torresi, A. Trzcinska, Y. X. Watanabe, and H. Yamaguchi, Eur. Phys. J. A **51**, 55 (2015).
[35] A. Gomez Camacho and E. F. Aguilera, Phys. Rev. C **90**, 064607 (2014).
[36] A. Gomez Camacho, N. Yu, H. Q. Zhang, P. R. S. Gomes, H. M. Jia, J. Lubian, and C. J. Lin, Phys. Rev. C **91**, 044610 (2015).
[37] J. J. Kolata, V. Guimarães, D. Peterson, P. Santi, R. White-Stevens, P. A. DeYoung, G. F. Peaslee, B. Hughey, B. Atalla, M. Kern, P. L. Jolivette, J. A. Zimmerman, M. Y. Lee, F. D. Becchetti, E. F. Aguilera, E. Martinez-Quiroz, and J. D. Hinnefeld, Phys. Rev. Lett. **81**, 4580 (1998).
[38] E. Martinez-Quiroz, E. F. Aguilera, D. Lizcano, P. Amador-Valenzuela, H. Garcia-Martinez, J. J. Kolata, A. Roberts, L. O. Lamm, G. Rogachev, V. Guimaraes, F. D. Becchetti, A. Villano, M. Ojaruega, M. Febbraro, Y. Chen, H. Jiang, P. A. DeYoung, and G. F. Peaslee, Phys. Rev. C **90**, 014616 (2014).
[39] R. Raabe, J. L. Sida, J. L. Charvet, N. Alamanos, C. Angulo, J. M. Casandjian, S. Courtin, A. Drouart, D. J. C. Durand, P. Figuera, A. Gillibert, S. Heinrich, C. Jouanne, V. Lapoux, A. Lepine-Szily, A. Musumarra, L. Nalpas, D. Pierroutsakou, M. Romoli, K. Rusek, and M. Trotta, Nature (London) **431**, 823 (2004).
[40] A. Lemasson, A. Shrivastava, A. Navin, M. Rejmund, N. Keeley, V. Zelevinsky, S. Bhattacharyya, A. Chatterjee, G.de France, B. Jacquot, V. Nanal, R. G. Pillay, R. Raabe, and C. Schmitt, Phys. Rev. Lett. **103**, 232701 (2009).
[41] R. Raabe, C. Angulo, J. L. Charvet, C. Jouanne, L. Nalpas, P. Figuera, D. Pierroutsakou, M. Romoli, and J. L. Sida, Phys. Rev. C **74**, 044606 (2006).
[42] C. Y. Wong, Phys. Rev. Lett. **31**, 766 (1973).
[43] C. Beck, F. A. Souza, N. Rowley, S. J. Sanders, N. Aissaoui, E. E. Alonso, P. Bednarczyk, N. Carlin, S. Courtin, A. Diaz-Torres, A. Dummer, F. Haas, A. Hachem, K. Hagino, F. Hoellinger, R. V. F. Janssens, N. Kintz, R. Liguori Neto, E. Martin, M. M. Moura, M. G. Munhoz, P. Papka, M. Rousseau, A. Sanchez i Zafra, O. Stezowski, A. A. Suaide, E. M. Szanto, A. Szanto de Toledo, S. Szilner, and J. Takahashi, Phys. Rev. C **67**, 054602 (2003).
[44] M. Ray, A. Mukherjee, M. K. Pradhan, Ritesh Kshetri, M. Saha Sarkar, R. Palit, I. Majumdar, P. K. Joshi, H. C. Jain, and B. Dasmahapatra, Phys. Rev. C **78**, 064617 (2008).
[45] A. Pakou, K. Rusek, N. Alamanos, X. Aslanoglou, M. Kokkoris, A. Lagoyannis, T. J. Mertzimekis, A. Musumarra, N. G. Nicolis, D. Pierroutsakou, and D. Roubos, Eur. Phys. J. A **39**, 187 (2009).
[46] M. Sinha, H. Majumdar, P. Basu, Su. Roy, R. Bhattacharya, M. Biswas, M. K. Pradhan, R. Palit, I. Mazumdar, and S. Kailas, Eur. Phys. J. **A 44**, 403 (2010).
[47] A. Di Pietro, P. Figuera, E. Strano, M. Fisichella, O. Goryunov, M. Lattuada, C. Maiolino, C. Marchetta, M. Milin, A. Musumarra, V. Ostashko, M. G. Pellegriti, V. Privitera, G. Randisi, L. Romano, D. Santonocito, V. Scuderi, D. Torresi, and M. Zadro, Phys. Rev. C **87**, 064614 (2013).
[48] M. Dasgupta, D. J. Hinde, K. Hagino, S. B. Moraes, P. R. S. Gomes, R. M. Anjos, R. D. Butt, A. C. Berriman, N. Carlin, C. R. Morton, J. O. Newton, and A. Szanto de Toledo, Phys. Rev. C **66**, 041602(R) (2002).
[49] A. Diaz-Torres, I. J. Thompson, and C. Beck, Phys. Rev. C **68**, 044607 (2003).
[50] V. Z. Maidikov, T. Glodariu, M. La Commara, M. Sandoli, C. Signorini, L. Costa, F. Soramel, R. Bonetti, A. De Rosa, M. Di Pietro, A. Guglielmetti, G. Inglima, B. Martin, M. Mazzocco, D. Pierroutsakou, M. Romoli, P. Scopel, and L. Stroe, Nucl. Phys. A **746**, 389c (2004).
[51] D. Pierroutsakou, B. Martin, T. Glodariu, M. Mazzocco, R. Bonetti, A. De Francesco, A. De Rosa, F. Farinon, A. Guglielmetti, G. Inglima, M. La Commara, M. Romoli, M. Sandoli, C. Signorini, F. Soramel, L. Stroe, and E. Vardaci, Eur. Phys. J. Spec. Top. **150**, 47 (2007).
[52] F. Farinon, T. Glodariu, M. Mazzocco, A. Battistella, R. Bonetti, L. Costa, A. De Rosa, A. Guglielmetti, G. Inglima, M. La Commara, V. Z. Maidikov, B. Martin, C. Mazzocchi, D. Pierroutsakou, M. Romoli, M. Sandoli, C. Signorini, F. Soramel, L. Stroe, and E. Vardaci, Nucl. Instrum. Methods **B266**, 4097 (2008).
[53] M. Mazzocco, F. Farinon, T. Glodariu, H. Geissel, A. Guglielmetti, N. Iwasa, M. La Commara, B. Martin, C. Mazzocchi, D. Pierroutsakou, M. Romoli, M. Sandoli, C. Signorini, F. Soramel,

L. Stroe, E. Vardaci, H. Weick, and M. Winkler, Nucl. Instrum. Methods **B 266**, 4665 (2008).

[54] M. Mazzocco, D. Torresi, E. Strano, A. Boiano, C. Boiano, L. Costa, T. Glodariu, A. Guglielmetti, M. L Commara, C. Parascandolo, D. Pierroutsakou, C. Signorini, F. Soramel, and L. Stroe, Nucl. Instrum. Methods **B317**, 223 (2013).

[55] E. Strano, A. Anastasio, M. Bettini, A. Boiano, C. Boiano, C. Cassese, L. Castellani, D. Corti, P. Di Meo, G. Galet, T. Glodariu, J. Grebosz, A. Guglielmetti, M. La Commara, C. Manea, M. Mazzocco, P. Molini, M. Nicoletto, C. Parascandolo, L. Parascandolo, D. Pierroutsakou, G. Pontoriere, L. Roscilli, C. Signorini, F. Soramel, L. Stroe, M. Tessaro, N. Toniolo, D. Torresi, and P. G. Zatti, Nucl. Instrum. Methods **B317**, 657 (2013).

[56] D. Pierroutsakou, A. Boiano, C. Boiano, P. Di Meo, M. La Commara, C. Manea, M. Mazzocco, M. Nicoletto, C. Parascandolo, C. Signorini, F. Soramel, E. Strano, N. Toniolo, D. Torresi, G. Tortone, A. Anastasio, M. Bettini, C. Cassese, L. Castellani, D. Corti, L. Costa, B. De Fazio, G. Galet, T. Glodariu, J. Grebosz, A. Guglielmetti, P. Molini, G. Pontoriere, R. Rocco, M. Romoli, L. Roscilli, M. Sandoli, L. Stroe, M. Tessaro, and P. G. Zatti, Nucl. Instrum. Methods **A 834**, 46 (2016).

[57] K. K. Olimov, K. Olimov, V. V. Lugovoi, P. I. Zarubin, S. L. Lutpullaev, A. K. Olimov, V. Sh. Navotny, U. U. Abdurakhmanov, D. A. Artemenkov, I. G. Zarubina, V. V. Rusakova, A. Arif, and I. Khan, Int. J. Mod. Phys. E **25**, 1650021 (2016).

[58] A. Gavron, Phys. Rev. C **21**, 230 (1980).

[59] R. Bass, Phys. Rev. Lett. **39**, 265 (1977).

[60] J. R. Huizenga and G. Igo, Nucl. Phys. **29**, 462 (1962).

[61] E. F. Aguilera, P. Amador-Valenzuela, E. Martinez-Quiroz, J. Fernandez-Arnaiz, J. J. Kolata, and V. Guimaraes, Phys. Rev. C **93**, 034613 (2016).

[62] L. McFadden and G. R. Satchler, Nucl. Phys. **84**, 177 (1966).

[63] G. R. Satchler, Nucl. Phys. **70**, 177 (1965).

[64] L. F. Canto, P. R. S. Gomes, J. Lubian, L. C. Chamon, and E. Crema, Nucl. Phys. A **821**, 51 (2009).

[65] G. V. Marti, P. R. S. Gomes, M. D. Rodriguez, J. O. Fernandez Niello, O. A. Capurro, A. J. Pacheco, J. E. Testoni, M. Ramirez, A. Arazi, I. Padron, R. M. Anjos, J. Lubian, and E. Crema, Phys. Rev. C **71**, 027602 (2005).

[66] K. Kalita, S. Verma, R. Singh, J. J. Das, A. Jhingan, N. Madhavan, S. Nath, T. Varughese, P. Sugathan, V. V. Parkar, K. Mahata, K. Ramachandran, A. Shrivastava, A. Chatterjee, S. Kailas, S. Barua, P. Basu, H. Majumdar, M. Sinha, R. Bhattacharya, and A. K. Sinha, Phys. Rev. C **73**, 024609 (2006).

[67] A. Pakou, K. Rusek, N. Alamanos, X. Aslanoglou, M. Kokkoris, A. Lagoyannis, T. J. Mertzimekis, A. Musumarra, N. G. Nicolis, D. Pierroutsakou, and D. Roubos, internal report, Nuclear Physic Laboratory, University of Ioannina, 2008 (unpublished), http://npl.physics.uoi.gr/preprints/internal_NPL08_1.pdf

[68] M. Sinha, H. Majumdar, R. Bhattacharya, P. Basu, S. Roy, M. Biswas, R. Palit, I. Mazumdar, P. K. Joshi, H. C. Jain, and S. Kailas, Phys. Rev. C **76**, 027603 (2007).

[69] M. Sinha, H. Majumdar, P. Basu, S. Roy, R. Bhattacharya, M. Biswas, M. K. Pradhan, and S. Kailas, Phys. Rev. C **78**, 027601 (2008).

[70] A. Pakou, E. Stiliaris, D. Pierroutsakou, N. Alamanos, A. Boiano, C. Boiano, D. Filipescu, T. Glodariu, J. Grebosz, A. Guglielmetti, M. La Commara, M. Mazzocco, C. Parascandolo, K. Rusek, A. M. Sanchez-Benitez, C. Signorini, O. Sgouros, F. Soramel, V. Soukeras, E. Strano, L. Stroe, N. Toniolo, D. Torresi, and K. Zerva, Phys. Rev. C **87**, 014619 (2013).

[71] P. R. Christensen and A. Winther, Phys. Lett. B **65**, 19 (1976).

[72] N. Keeley, K. W. Kemper, and K. Rusek, Phys. Rev. C **66**, 044605 (2002).

[73] J. Cook, Nucl. Phys. A **388**, 153 (1982).

[74] S. Cohen and D. Kurath, Nucl. Phys. A **101**, 1 (1967).

[75] M. C. Mermaz, C. A. Whitten, Jr., J. W. Champlin, A. J. Howard, and D. A. Bromley, Phys. Rev. C **4**, 1778 (1971).

[76] C. A. Whitten, Jr., M. C. Mermaz, and D. A. Bromley, Phys. Rev. C **1**, 1455 (1970).

[77] C. W. Woods, N. Stein, and J. W. Sunier, Phys. Rev. C **17**, 66 (1978).

[78] D. Y. Pang, P. Roussel-Chomaz, H. Savajols, R. L. Varner, and R. Wolski, Phys. Rev. C **79**, 024615 (2009); **81**, 019902(E) (2010).

[79] B. Buck and A. C. Merchant, J. Phys. G **14**, L211 (1988).

[80] T. Madhusoodhanan, S. Mandal, R. Shyam, M. R. Rao, M. T. Lagare, N. G. Puttaswamy, A. Mandal, D. K. Avasthi, and S. K. Datta, J. Phys. G **25**, 1897 (1999).

[81] A. Shrivastava, A. Navin, A. Diaz-Torres, V. Nanal, K. Ramachandran, M. Rejmund, S. Bhattacharyya, A. Chatterjee, S. Kailas, A. Lemasson, R. Palit, V. V. Parkar, R. G. Pillay, P. C. Rout, and Y. Sawant, Phys. Lett. B **718**, 931 (2013).

[82] I. J. Thompson, M. A. Nagarajan, J. S. Lilley, and M. J. Smithson, Nucl. Phys. A **505**, 84 (1989).